KEY-GRAPH TRANSFORMER FOR IMAGE RESTORATION

Anonymous authors
Paper under double-blind review

ABSTRACT

It is widely acknowledged that capturing non-local information among pixels within one input image is crucial for effective image restoration (IR). However, fully incorporating such global cues into transformer-based methods can be computationally expensive, mainly when dealing with large input images or patches. Furthermore, it is assumed that the attention mechanism within the transformer considers numerous unnecessary global cues of the pixels from unrelated objects or regions. In response to these challenges, we introduce the Key-Graph Transformer (KGT) for IR in this paper. Specifically, KGT treats image features within a given window as the nodes of a graph. Instead of establishing connections among all the nodes, the proposed Key-Graph Constructor creates a sparse yet representative Key-Graph that flexibly connects only the essential nodes. Then the Key-Graph Attention Block is proposed within each KGT layer to conduct the self-attention operation guided by the Key-Graph only among selected nodes with linear computational complexity. Extensive experimental results validate that the proposed KGT outperforms state-of-the-art methods on various benchmark datasets, quantitatively and qualitatively.

1 INTRODUCTION

Image restoration (IR), a fundamental task in the realm of low-level computer vision, is dedicated to the improvement of images that have been compromised by various factors such as noise, blur, or other forms of distortion. The central aim of image restoration is to reconstruct a cleaner, visually more appealing version of the original image, thus facilitating a more effective analysis and interpretation. This capability finds diverse applications, including information recovery (such as retrieving obscured data in medical imaging, surveillance, and satellite imagery) and supporting downstream vision tasks like object detection, recognition, and tracking Sezan & Stark (1982); Molina et al. (2001). Despite significant advancements in recent years, it is noteworthy that current popular image restoration methods still face challenges in effectively handling complex distortions or preserving/recovering essential image details Li et al. (2023a). In order to recover high-quality images, the rich information exhibited in the degraded counterparts needs to be exquisitely explored.

For IR in modern computer vision systems, the de-facto representative networks are mainly built based on three fundamental architectural paradigms, *i.e.,* the convolutional neural networks (CNNs) LeCun et al. (1998); Zamir et al. (2021), Vision Transformers (ViTs) Vaswani et al. (2017); Dosovitskiy et al. (2020) and the Multilayer perceptrons (MLPs) Bishop & Nasrabadi (2006); Tu et al. (2022). The input image/image patches are treated as a regular grid of pixels in the Euclidean space for CNNs or a sequence of patches for ViTs and MLPs. However, the degraded input images usually contain irregular and complex objects. These architectural choices perform admirably in specific scenarios characterized by regular or well-organized object boundaries but have limitations when applied to images with more flexible and complex geometrical contexts.

Besides the above-mentioned limitations of how they treat data, CNNs are struggling to model the long-range dependencies because of their limited receptive field. Though ViTs have been validated as highly effective in capturing the long-range relation among pixels with the multi-head self-attention mechanism (MSA) Vaswani et al. (2017); Dosovitskiy et al. (2020); Ren et al. (2023a), their computational complexity increases quadratically with respect to spatial resolution. Similarly, MLPs are not trivial to be applied to high-resolution input spatial-wise, which largely reduces the ability of MLPs to maintain the locality among the neighbor pixels. To overcome these limitations, recent methods investigate strategies for complexity reduction. One common approach is to implement MSA within local image regions using the SWIN-Transformer architecture design Liang et al. (2021); Li et al. (2023a). However, these designs treat input still as sequences, which hinders effective context aggregation within local neighborhoods and struggles to capture inherent connections among irregular objects. Additionally, an earlier study Zontak & Irani (2011) highlights that smooth image contents occur more frequently than complex image details, suggesting the need for differentiated treatment for different contents.

In this paper, we introduce a novel approach, the Key-Graph Transformer (KGT), to address the aforementioned limitations using the SWIN Liu et al. (2021) architecture. Our method comprises two core components: a K-nearest neighbors (KNN) based Key-Graph Constructor and a Key-Graph Transformer layer with a novel Key-Graph Attention block integrated. Specifically, starting with the input feature obtained from the convolutional feature extractor within one window, we treat each of them as a node representation of a graph. Since capturing long-range dependencies among all nodes can be highly computationally demanding, we selectively choose topK nodes based on the proposed Key-Graph constructor rather than establishing connections between all possible nodes. In particular, we propose a random topK strategy during training instead of a fixed topK value. This leads to a sparse yet representative graph that connects only the essential neighbor nodes, which makes our method achieve the same receptive field as previous transformer-based methods while effectively maintaining lower computational costs. The criteria for selecting these representative nodes are determined by the self-similarity calculated at the beginning of each KGT layer. Then the chosen nodes undergo processing by all the successive Key-Graph transformer layers shown in Fig. 1. It's worth noting that the implementation of the Key-Graph attention block within each KGT layer is achieved in three manners (*i.e.,* the Triton Dao et al. (2022), torch-mask, and torch-gather), which will be discussed in our ablation studies. Based on these two components, the information that exists in all the selected nodes is well-aggregated and updated.

In summary, our main contributions can be categorized as follows:

1. We propose a Key-Graph constructor that provides a sparse yet representative Key-Graph with the most relevant K nodes considered, which works as a reference for the subsequent attention layer, facilitating more efficient attention operations.
2. Based on the constructed Key-Graph, we introduce a Key-Graph Transformer layer with a novel Key-Graph attention block integrated. Notably, the computational complexity can be significantly reduced from quadratic to linear when compared to conventional attention operations.
3. Based on both the Key-Graph constructor and the Key-Graph Transformer layer, we propose a Key-Graph Transformer (KGT) for image restoration. Extensive experimental results show that the proposed KGT achieves state-of-the-art performance on 6 IR tasks.

2 Related Work

Image Restoration (IR), as a long-standing ill-posed inverse problem, is designed to reconstruct the high-quality image from the corresponding degraded counterpart. It has been brought to various real-life scenarios due to its valuable application property Richardson (1972); Banham & Katsaggelos (1997); Li et al. (2023b). Initially, IR was addressed through model-based solutions, involving the search for solutions to specific formulations. However, with the remarkable advancements in deep neural networks, learning-based approaches have gained increasing popularity. These approaches have been explored from various angles, encompassing both regression-based Lim et al. (2017); Liang et al. (2021); Chen et al. (2021b); Li et al. (2023a) pipelines and generative model-based pipelines Gao et al. (2023); Wang et al. (2023); Luo et al. (2023); Yue et al. (2023). In this paper, our primary focus is to investigate IR within the context of the regression-based pipeline.

Non-local Priors Modeling in IR. Tradition model-based IR methods reconstruct the image by regularizing the results (*e.g.*, Tikhonov regularization Golub et al. (1999)) with formulaic prior knowledge of natural image distribution. However, it's challenging for these model-based methods to recover realistic detailed results with hand-designed priors. Besides, some other classic method finds that self-similarity is an effective prior which leads to an impressive performance Buades et al. (2005); Dabov et al. (2007). Apart from the traditional methods, the non-local prior also has been uti-

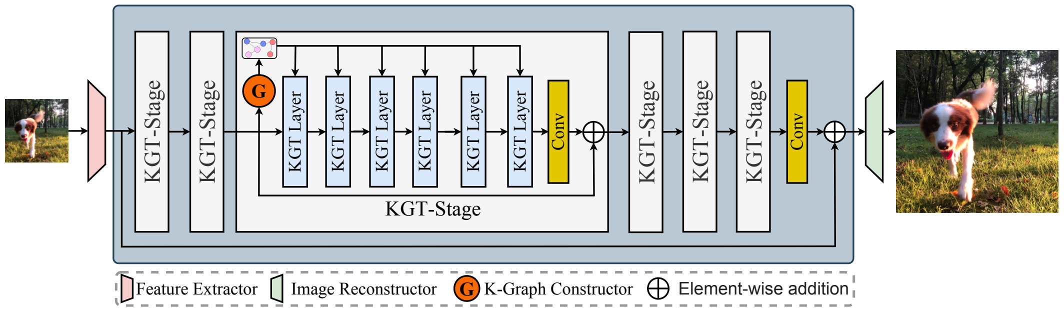

Figure 1: The architecture of the proposed Key-Graph Transformer (KGT) for Image Restoration. KGT mainly consists of a feature extractor, the main body of the proposed KGT (The main body here is for SR, while the U-shaped structure is used for other IR tasks), and an image reconstructor.

lized in modern deep learning networks Liu et al. (2018); Wang et al. (2018); Li et al. (2023a); Zhang et al. (2019b), and it was usually captured by the self-attention mechanism. Especially, KiT Lee et al. (2022) proposed to increase the non-local connectivity between patches of different positions via a KNN matching to better capture the non-local relations between the base patch and other patches in every attention operation, this brings more extra computation costs. DRSformer Chen et al. (2023) proposed a topK selection strategy that chooses the most relevant tokens to model the non-local priors for draining after each self-attention operation without reducing the computation complexity. The effectiveness of non-local priors has been widely validated in various recent transformer-based IR methods Liang et al. (2021); Zamir et al. (2022); Li et al. (2023a).

Graph-Perspective Solutions for IR. Graph operations are usually used to deal with irregular data structures such as point clouds Wang et al. (2019); Li et al. (2021b), social networks Myers et al. (2014), or protein desins Ingraham et al. (2019). Recently, graph-based methods were also adapted to process the input image/patches in a more flexible manner Gori et al. (2005); Scarselli et al. (2008); Mou et al. (2021); Han et al. (2022); Jiang et al. (2023) on various IR tasks, like facial expression restoration Liu et al. (2020), image denoising Simonovsky & Komodakis (2017), and artifact reduction Mou et al. (2021). However, most of the previous graph-based solutions for IR mainly extend from graph neural networks (GNNs), which mainly focus on very close neighbor nodes. Merely increasing the depth or width of GNNs proves inadequate for expanding receptive fields Xu et al. (2018), as larger GNNs often face optimization challenges like vanishing gradients and over-smoothing representation. Jiang et al. (2023) construct the graph with transformer-based architecture but in a very expensive manner where each node is connected to all other nodes. In this paper, we introduce a novel approach that integrates graph properties into ViTs by employing a Key-Graph for the efficient capture of effective non-local priors in Image Restoration (IR) tasks.

3 METHODOLOGY

The overall architecture of the proposed Key-Graph Transformer (KGT) is shown in Fig. 1. Unlike conventional approaches that treat input features after the convolutional feature extractor as a regular grid of pixels in Euclidean space (typical in CNNs) or as a sequence of patches (common in ViTs and MLPs), our method adopts a more flexible approach based on graph representation. To be specific, the proposed KGT focuses on enhancing the efficiency of representation learning in a multi-stage manner. The graph structure is shared within each KGT stage and can be dynamically updated at the beginning of each KGT stage, which leads to a sparse yet highly effective node representation. Before delving into our proposed method, we begin by offering a succinct overview of the foundational concepts of graph transformers in the preliminary section (Section 3.1). We then ensure the efficiency of graph updating by introducing the Key-Graph constructor (Section 3.2). Simultaneously, we attain the effectiveness of node feature aggregation by employing the Key-Graph Transformer Layer (Section 3.3) in each stage of the KGT.

3.1 PRELIMINARY: GRAPH TRANSFORMER.

In conventional vision transformers, graph nodes are typically assigned based on feature patches, and graph edges are usually represented by inferring similarities among nodes using a self-attention

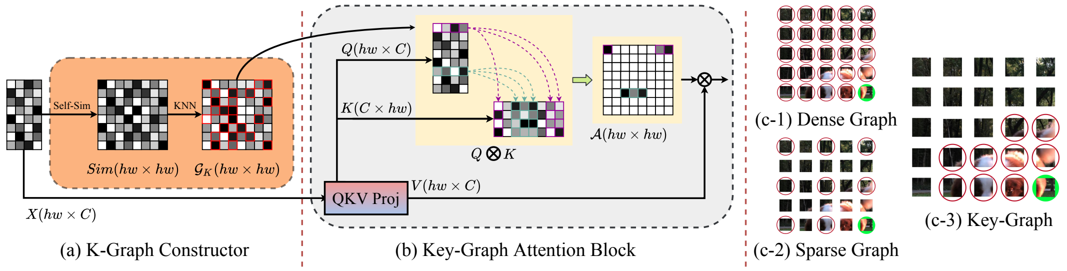

Figure 2: (a): The illustration of Key-Graph Constructor. (b): The proposed Key-Graph Attention Block within each KGT Layer. (c): The depiction of the difference among dense graph attention c-1, sparse graph attention c-2, and the proposed Key-Graph attention c-3.

mechanism Vaswani et al. (2017). Specifically, given the low-level input feature $F_{in} \in \mathbb{R}^{H \times W \times C}$, where H, W, and C denote the height, the width, and the numbers of channels of the given feature, respectively. F_{in} is split into N feature patches and we get the node feature representation $X = \{x_i | x_i \in \mathbb{R}^{hw \times c}, i = 1, 2, 3, ..., N\}$, where h, w, and c denote the height, the width, and the feature dimension of each patched feature. These features can be considered to be an unordered set of nodes. For each node x_i, an edge e_{ji} can be added from x_j to x_i from all the neighbors of x_i in X. Thus, a graph $\mathcal{G}$ is naturally constructed and can be represented by the corresponding adjacency matrix $\mathcal{A} = \{e_{ji}\} \in \mathbb{R}^{N \times N}$.

In order to get $\mathcal{A}$, we begin by linearly projecting X into Query (Q), Key (K), and Value (V) matrices (note that V will be used to conduct the node feature aggregation with the help of $\mathcal{A}$ later), which are denoted as $Q = X\mathbf{W}_Q$, $K = X\mathbf{W}_K$, and $V = X\mathbf{W}_V$, respectively. Here, $\mathbf{W}_{Q/K/V}$ represents the learnable projection weights. The calculation of $\mathcal{A}$ is performed as follows:

$$\mathcal{A}_{ij} = softmax(QK^T/\sqrt{d}) = \frac{exp(Q_i K_j/\sqrt{d})}{\sum_{k \in X_i} exp(Q_i K_k/\sqrt{d})}, j \in X_i \tag{1}$$

where d represents the dimension of Q/K. Then the node feature can be aggregated to $\hat{x_i}$ by:

$$\hat{x_i} = \mathcal{A}_{ij} \cdot V_i \tag{2}$$

Since we have adopted the SWIN transformer Liu et al. (2021) as the basic architecture that conducts the window-wise attention, all the operations within each window are similar. To streamline our explanation, we select a single window for illustration when discussing the Key-Graph Constructor and the proposed Key-Graph Transformer layer. Notably, notations such as F_{in} and X are all window-size adapted for clarity.

3.2 Key-Graph Constructor

The goal of the proposed Key-Graph constructor is to construct a sparse yet representative graph $\mathcal{G}_K$ at the beginning of each KGT stage. Specifically, given node representation X of F_{in}, an initial fully connected Graph $\mathcal{G}$ is constructed by calculating the self-similarity of X via dot product operation. As a result, the corresponding adjacency metrics $\mathcal{A}$ can be achieved:

$$\mathcal{A} = sim(i, j) = x_i \cdot x_j^T, \tag{3}$$

which describes the correlation among all the nodes, and a higher similarity value indicates a higher correlation between two nodes. However, in this context, $\mathcal{A}$ represents a fully connected graph, wherein all nodes x_j within X are included in the connectivity of the destination node x_i, irrespective of the degree of relatedness between x_i and x_j (*e.g.*, Fig. 2 (c-1) describes such a case that the green dog patch node at the bottom right corner is also connected to all other nodes with a red circle marked. Best viewed by zooming.).

To mitigate the side effects of nodes with low correlation (*e.g.,* the tree-related nodes at the upper left part) for the destination dog node, we propose to keep only K highly related nodes of the destination node x_i and exclude the remaining nodes with low correlation. This is achieved under the guidance

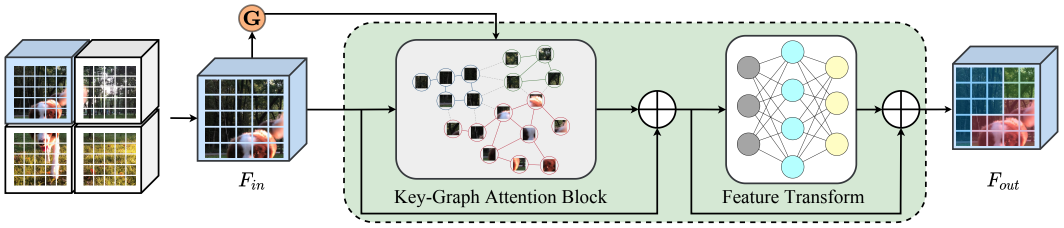

Figure 3: The framework of the proposed Key-Graph Transformer Layer.

of the similarity value from $\mathcal{A}$ as follows:

$$\mathcal{A}_K(i,j) = \begin{cases} \mathcal{A}(i,j), & \mathcal{A}(i,j) \geq sim(i,)_K \\ 0, & else \end{cases} \tag{4}$$

where $sim(i,)_K$ denotes the K_{th} largest connective value of node x_i with its corresponding node. As a result, once $\mathcal{A}_K$ is achieved, we get a sparse yet representative Key-Graph $\mathcal{G}_K$ which contains only the edge connection among the destination node (*e.g.,* the green dog node) and the other nodes with high correlation (*e.g.,* dog-related nodes. An example is illustrated in Fig. 2 (c-3)).

Owing to the permutation-invariant property inherent in both the MSA and the FFN within each transformer layer Vaswani et al. (2017); Lee et al. (2019), the KGT layer consistently produces identical representations for nodes that share the same attributes, regardless of their positions or the surrounding structures within the graph Chen et al. (2022a). In other words, nodes at the same spatial location are consistently connected to other nodes possessing the same attributes as they traverse through the various layers within the same KGT stage. This enables our Key-Graph $\mathcal{G}_K$ to act as a reference for each attention block in the subsequent KGT layers within each KGT stage, facilitating more efficient attention operations. This is different from the sparse graph (illustrated in Fig. 2 (c-2)) that only activates the nodes in a fixed coordinate of a given feature map Zhang et al. (2023b).

3.3 Key-Graph Transformer Layer

The proposed Key-Graph Transformer Layer is shown in Fig. 3, which consists of a Key-Graph attention block together with an FFN for the node feature aggregation. Fig. 2 (b) shows the detailed workflow of the proposed Key-Graph attention block. Initially, the node features X undergo a linear projection into Q, K, and V. Then for each node in x_i in Q, instead of calculating the self-attention with all the nodes x_j in K, we choose only topK nodes in K where j denotes only the index of the nodes with high correlation to the given destination node. The selection is guided by the Key-Graph $\mathcal{G}_K$. We intuitively show such a process in Fig. 2 (a) and (b), and formulate the selection process as $K_K = select(topK, \mathcal{G}_K)$. Then the spare yet representative adjacency matrix $\mathcal{A}_K$ is can be obtained by:

$$\mathcal{A}_K = softmax_K(QK_K^T/\sqrt{d}), \tag{5}$$

which captures the pair-wise relation between each destination node $x_i, (i = 1, 2, ..., hw)$ in Q with only the nodes that are semantically related to the given x_i. For other nodes apart from the selected K nodes, we keep their position in their corresponding places without any computation. This is different from the conventional self-attention operation which calculates the relation of each node in Q and all nodes in K (The difference between c-1 and c-3 in Fig. 2). Meanwhile, the proposed method is also different from the sparse attention used in Zhang et al. (2023b) where the position of the nodes that need to be collected is always fixed (The difference between c-2 and c-3 in Fig. 2). Conversely, the proposed Key-Graph attention block not only significantly reduces the computational complexity from $\mathcal{O}((hw)^2)$ to $\mathcal{O}((hw) \times K)$, where $K < hw$, but also provides a more flexible approach to capturing semantically highly related nodes.

Note that since the dimension of the select $\mathcal{G}_K$ only contains topK nodes, this leads to a dimension mismatch problem for the conventional self-attention mechanism. As a remedy, we tried three different manners for the detailed implementation, *i.e.,* (i) *Triton*, (ii) *Torch-Gather*, and (iii) *Torch-Mask*. Specifically, (i) is based on FlashAttention Dao et al. (2022), and parallel GPU kernels are called for the nodes. (ii) means that we use the 'torch.gather()' function in PyTorch to choose the

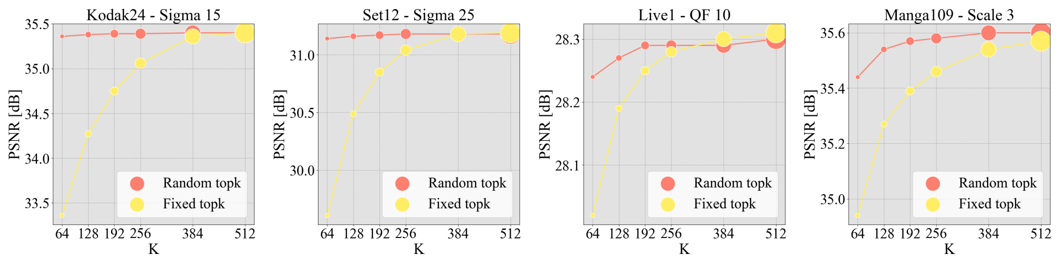

(a) Color image denoising on Kodak24, $\sigma = 15$.
(b) Grayscale image denoising on Set12, $\sigma = 25$
(c) Color image JPEG CAR on Live1, $QF = 10$.
(d) SR with KGT-B on Manga109, upscaler $\times 3$.

Figure 4: Ablation study on the impact of K. The size of the circle denotes the FLOPs.

corresponding Q_{gather} and K_{gather} based on $\mathcal{G}_K$, then the attention operation shown in Eq. 5 is conducted between Q_{gather} and K_{gather}. (iii) denotes that we keep only the value of selected nodes of $\mathcal{A}_K$ and omitting other nodes with low correlation via assigning those values to $-\infty$ guided by $\mathcal{G}_K$. We will discuss the pros and cons of these manners in Sec. 4.1.

Finally, as the phenomenon of over-smoothing is prevalent in graph-structured data, it becomes particularly pronounced in deep models Chen et al. (2020); Keriven (2022). To relieve the over-smoothing phenomenon and encourage the node feature transformation capacity, we aggregate the node feature by an FFN in a residual connection manner. This process can be formalized as follows:

$$Z = FFN(X + \mathcal{A}_K V), \tag{6}$$

where $Z = \{z_i | z_i \in \mathbb{R}^{hw \times c}, i = 1, 2, 3, ..., N\}$ is the aggregated node feature.

4 Experiments

In this section, we first analyze two important aspects of the proposed KGT, followed by extensive experiments on **6** IR tasks, which include JPEG compression artifact reduction (CAR), image denoising, demosaicking, IR in adverse weather conditions (AWC), image super-resolution (SR), and image deblurring. More details about the training protocols, the training/testing dataset, and additional visual results are shown in the *supplementary material (Supp. Mat.)*. In addition, the best and the second-best quantitative results in all tables are reported in red and blue, respectively.

4.1 Ablation Study

Extensive ablation experiments are conducted for the following two essential explorations:

The Impact of the K in Key-Graph Constructor. Two sets of experiments are conducted to study the influence of hyper-parameter K. In the first set, K was held constant at 512 throughout the training process, while in the second set, K was randomly sampled from the values $[64, 128, 192, 256, 384, 512]$. It's important to note that for both sets, K was configured to the specified value during the inference phase. Besides the truth that the computational complexity grows linearly with K, there are two interesting phenomena that can be observed from the results shown in Fig. 4, *i.e.,* (1). The randomly sampled strategy has a very stable and better performance compared to the fixed K manner especially when the K is fixed to a small number (*i.e.*, 64, 128, 256). (2) The PSNR can largely increase with the increase of K in a fixed manner. We conclude that a random sampled strategy is more general and stable. It can also make the inference process more flexible regarding different computation resources. More ablation results can be found in our *Supp. Mat.* about the effect of the noise level and quality factor for denoising and JPEG CAR.

The impact of the implementation of Key-Graph Attention is assessed in terms of (i) *Triton*, (ii) *Torch-Gather*, and (iii) *Torch-Mask* under different numbers of N (various from 512 to 8192) and K (various from 32 to 512). The results of the GPU memory footprint are shown in Tab. 3, which indicate that *Torch-Gather* brings no redundant computation while requiring a large memory footprint. Though *Torch-Mask* brings the GPU memory increase, the increment is affordable compared to *Torch-Gather* and also very easy to implement. *Triton* can largely save the GPU memory while at the cost of slow inference and difficult implementation for the back-propagation process. To

Table 1: ***Grayscale image JPEG compression artifact removal*** results. †A single model is trained to handle multiple quality factors.

Set	QF	JPEG		†DnCNN3		†DRUNet		†KGT (Ours)		GRL-S		SwinIR		ART		CAT		KGT (Ours)	
		PSNR	SSIM	PSNR	SSIM	PSNR	SSIM	PSNR	SSIM	PSNR	SSIM	PSNR	SSIM	PSNR	SSIM	PSNR	SSIM	PSNR	SSIM
Classic5	10	27.82	0.7600	29.40	0.8030	30.16	0.8234	30.26	0.8240	30.20	0.8286	30.27	0.8249	30.27	0.8258	30.26	0.8250	30.36	0.8267
	20	30.12	0.8340	31.63	0.8610	32.39	0.8734	32.52	0.8740	32.49	0.8776	32.52	0.8748	-	-	32.57	0.8754	32.58	0.8748
	30	31.48	0.8670	32.91	0.8860	33.59	0.8949	33.74	0.8955	33.72	0.8985	33.73	0.8961	33.74	0.8964	33.77	0.8964	33.77	0.8958
	40	32.43	0.8850	33.77	0.9000	34.41	0.9075	34.55	0.9078	34.53	0.9107	34.52	0.9082	34.55	0.9086	34.58	0.9087	34.57	0.9080
LIVE1	10	27.77	0.7730	29.19	0.8120	29.79	0.8278	29.84	0.8323	29.82	0.8323	29.86	0.8287	29.89	0.8300	29.89	0.8295	29.92	0.8360
	20	30.07	0.8510	31.59	0.8800	32.17	0.8899	32.23	0.8949	32.22	0.8930	32.25	0.8909	-	-	32.30	0.8913	32.28	0.8950
	30	31.41	0.8850	32.98	0.9090	33.59	0.9166	33.65	0.9213	33.65	0.9190	33.69	0.9174	33.71	0.9178	33.73	0.9177	33.69	0.9201
	40	32.35	0.9040	33.96	0.9250	34.58	0.9312	34.65	0.9329	34.64	0.9331	34.67	0.9317	34.70	0.9322	34.72	0.9320	34.67	0.9345
Urban100	10	26.33	0.7816	28.54	0.8484	30.31	0.8745	30.81	0.8885	30.70	0.8875	30.55	0.8835	30.87	0.8894	30.81	0.8866	31.15	0.8941
	20	28.57	0.8545	31.01	0.9050	32.81	0.9241	33.33	0.9266	33.24	0.9270	33.12	0.9190	-	-	33.38	0.9269	33.51	0.9272
	30	30.00	0.9013	32.47	0.9312	34.23	0.9414	34.74	0.9446	34.67	0.9430	34.58	0.9417	34.81	0.9442	34.81	0.9449	34.84	0.9462
	40	31.06	0.9215	33.49	0.9412	35.20	0.9547	35.69	0.9447	35.62	0.9519	35.50	0.9515	35.73	0.9553	35.73	0.9511	35.75	0.9550

Table 2: ***Color image JPEG compression artifact removal*** results. †A single model is trained to handle multiple quality factors.

Set	QF	JPEG		†QGAC		†FBCNN		†DRUNet		†KGT (Ours)		SwinIR		GRL-S		KGT (Ours)	
		PSNR	SSIM	PSNR	SSIM	PSNR	SSIM	PSNR	SSIM	PSNR	SSIM	PSNR	SSIM	PSNR	SSIM	PSNR	SSIM
LIVE1	10	25.69	0.7430	27.62	0.8040	27.77	0.8030	27.47	0.8045	28.19	0.8146	28.06	0.8129	28.13	0.8139	28.31	0.8176
	20	28.06	0.8260	29.88	0.8680	30.11	0.8680	30.29	0.8743	30.53	0.8781	30.44	0.8768	30.49	0.8776	30.61	0.8792
	30	29.37	0.8610	31.17	0.8960	31.43	0.8970	31.64	0.9020	31.89	0.9051	31.81	0.9040	31.85	0.9045	31.94	0.9058
	40	30.28	0.8820	32.05	0.9120	32.34	0.9130	32.56	0.9174	32.81	0.9201	32.75	0.9193	32.79	0.9195	32.85	0.9204
BSDS500	10	25.84	0.7410	27.74	0.8020	27.85	0.7990	27.62	0.8001	28.25	0.8076	28.22	0.8075	28.26	0.8083	28.37	0.8102
	20	28.21	0.8270	30.01	0.8690	30.14	0.8670	30.39	0.8711	30.55	0.8738	30.54	0.8739	30.57	0.8746	30.63	0.8750
	30	29.57	0.8650	31.330	0.8980	31.45	0.8970	31.73	0.9003	31.90	0.9026	31.90	0.9025	31.92	0.9030	31.96	0.9035
	40	30.52	0.8870	32.25	0.9150	32.36	0.9130	32.66	0.9168	32.84	0.9190	32.84	0.9189	32.86	0.9192	32.88	0.9193

Table 3: GPU memory footprint of different implementations of the key-graph attention block. N is the number of tokens and K is the number of nearest neighbors.

N	Triton	Torch-Gather	Torch-Mask
512	0.27 GB	0.66 GB	0.36 GB
1024	0.33 GB	1.10 GB	0.67 GB
2048	0.68 GB	2.08 GB	1.91 GB
4096	2.61 GB	4.41 GB	6.83 GB
8192	10.21 GB	10.57 GB	26.42 GB
K	Triton	Torch-Gather	Torch-Mask
32	5.51 GB	15.00 GB	13.68 GB
64	5.82 GB	27.56 GB	13.93 GB
128	6.45 GB	OOM	14.43 GB
256	7.70 GB	OOM	15.43 GB
512	10.20 GB	OOM	17.43 GB

Table 4: ***Single-image motion deblurring*** results. GoPro dataset Nah et al. (2017) is used for training.

Method	**GoPro**		**HIDE**		Average	
	PSNR↑	SSIM↑	PSNR↑	SSIM↑	PSNR↑	SSIM↑
DeblurGAN Kupyn et al. (2018)	28.70	0.858	24.51	0.871	26.61	0.865
Nah *et al.* Nah et al. (2017)	29.08	0.914	25.73	0.874	27.41	0.894
DeblurGAN-v2 Kupyn et al. (2019)	29.55	0.934	26.61	0.875	28.08	0.905
SRN Tao et al. (2018)	30.26	0.934	28.36	0.915	29.31	0.925
Gao *et al.* Gao et al. (2019)	30.90	0.935	29.11	0.913	30.01	0.924
DBGAN Zhang et al. (2020)	31.10	0.942	28.94	0.915	30.02	0.929
MT-RNN Park et al. (2020)	31.15	0.945	29.15	0.918	30.15	0.932
DMPHN Zhang et al. (2019a)	31.20	0.940	29.09	0.924	30.15	0.932
Suin *et al.* Suin et al. (2020)	31.85	0.948	29.98	0.930	30.92	0.939
CODE Zhao et al. (2023)	31.94	-	29.67	-	30.81	-
SPAIR Purohit et al. (2021)	32.06	0.953	30.29	0.931	31.18	0.942
MIMO-UNet+ Cho et al. (2021)	32.45	0.957	29.99	0.930	31.22	0.944
IPT Chen et al. (2021a)	32.52	-	-	-	-	-
MPRNet Zamir et al. (2021)	32.66	0.959	30.96	0.939	31.81	0.949
KiT Lee et al. (2022)	32.70	0.959	30.98	0.942	31.84	0.951
Restormer Zamir et al. (2022)	32.92	0.961	31.22	0.942	32.07	0.952
Ren *et al.* Ren et al. (2023b)	33.20	0.963	30.96	0.938	32.08	0.951
KGT (ours)	33.44	0.964	31.05	0.941	32.25	0.953

optimize the efficiency of the proposed KGT, we recommend employing *Torch-Mask* during training and *Triton* during inference, striking a balance between the efficiency and the GPU memory requirement.

4.2 Evaluation of KGT on Various IR Tasks

Evaluation on JPEG Compression Artifact Reduction. For JPEG CAR, the experiments for both grayscale and color images are conducted with four image quality factors ranging from 10 to 40 under two experimental settings (*i.e.,* a single model is trained to handle multiple quality factors, and each model for each image quality). The quantitative results shown in Tab. 1 validate that the KGT outperforms all other methods like DnCNN-3 Zhang et al. (2017), DRUNet Zhang et al. (2021), GRL-S Li et al. (2023a), SwinIR Liang et al. (2021), ART Zhang et al. (2023b), and CAT Chen et al. (2022b) under both settings. Besides, the results for color images in Tab. 2 also show that our KGT achieves the best results on all the test sets and quality factors among all compared methods like QGAC Ehrlich et al. (2020), FBCNN Jiang et al. (2021), DRUNet, SwinIR, and GRL-S. The visual comparisons in the *Supp. Mat.* further support the effectiveness of the proposed KGT.

Table 5: ***Color and grayscale image denoising*** results. Model complexity and prediction accuracy are shown for better comparison. †A single model is trained to handle multiple noise levels.

Method	# P	Color									Grayscale								
		CBSD68			McMaster			Urban100			Set12			BSD68			Urban100		
		σ=15	σ=25	σ=50	σ=15	σ=25	σ=50	σ=15	σ=25	σ=50	σ=15	σ=25	σ=50	σ=15	σ=25	σ=50	σ=15	σ=25	σ=50
†DnCNN	0.56	33.90	31.24	27.95	33.45	31.52	28.62	32.98	30.81	27.59	32.67	30.35	27.18	31.62	29.16	26.23	32.28	29.80	26.35
†FFDNet	0.49	33.87	31.21	27.96	34.66	32.35	29.18	33.83	31.40	28.05	32.75	30.43	27.32	31.63	29.19	26.29	32.40	29.90	26.50
†DRUNet	32.64	34.30	31.69	28.51	35.40	33.14	30.08	34.81	32.60	29.61	33.25	30.94	27.90	31.91	29.48	26.59	33.44	31.11	27.96
†Restormer	26.13	34.39	31.78	28.59	35.55	33.31	30.29	35.06	32.91	30.02	33.35	31.04	28.01	31.95	29.51	26.62	33.67	31.39	28.33
†KGT (Ours)	25.82	34.42	31.78	28.57	35.65	33.40	30.34	35.37	33.26	30.41	33.47	31.16	28.12	31.95	29.49	26.54	34.05	31.84	28.83
DnCNN	0.56	33.90	31.24	27.95	33.45	31.52	28.62	32.98	30.81	27.59	32.86	30.44	27.18	31.73	29.23	26.23	32.64	29.95	26.26
RNAN	8.96	-	-	28.27	-	-	29.72	-	-	29.08	-	-	27.70	-	-	26.48	-	-	27.65
IPT	115.33	-	-	28.39	-	-	29.98	-	-	29.71	-	-	-	-	-	-	-	-	-
EDT-B	11.48	34.39	31.76	28.56	35.61	33.34	30.25	35.22	33.07	30.16	-	-	-	-	-	-	-	-	-
DRUNet	32.64	34.30	31.69	28.51	35.40	33.14	30.08	34.81	32.60	29.61	33.25	30.94	27.90	31.91	29.48	26.59	33.44	31.11	27.96
SwinIR	11.75	34.42	31.78	28.56	35.61	33.20	30.22	35.13	32.90	29.82	33.36	31.01	27.91	31.97	29.50	26.58	33.70	31.30	27.98
Restormer	26.13	34.40	31.79	28.60	35.61	33.34	30.30	35.13	32.96	30.02	33.42	31.08	28.00	31.96	29.52	26.62	33.79	31.46	28.29
Xformer	25.23	34.43	31.82	28.63	35.68	33.44	30.38	35.29	33.21	30.36	33.46	31.16	28.10	31.98	29.55	26.65	33.98	31.78	28.71
KGT (Ours)	25.82	34.43	31.79	28.60	35.65	33.43	30.38	35.38	33.29	30.51	33.48	31.18	28.14	31.97	29.52	26.53	34.09	31.87	28.86

Table 6: ***Image Restoration in adverse weather conditions***.

Type	Test1 (rain+fog)		SnowTest100k-L		RainDrop	
	Method	PSNR	Method	PSNR	Method	PSNR
Task Specific	pix2pix	19.09	DesnowNet	27.17	Attn. GAN	30.55
	HRGAN	21.56	JSTASR	25.32	Quan *et al.*	31.44
	SwinIR	23.23	SwinIR	28.18	SwinIR	30.82
	MPRNet	21.90	DDMSNET	28.85	CCN	31.34
Multi Task	All-in-One	24.71	All-in-One	28.33	All-in-One	31.12
	TransWeather	27.96	TransWeather	28.48	TransWeather	28.84
	KGT (Ours)	29.57	KGT (Ours)	30.76	KGT (Ours)	30.82

Table 7: ***Image demosaicking*** results.

Datasets	Kodak	McMaster
Matlab	35.78	34.43
MMNet Kokkinos et al. (2019)	40.19	37.09
DDR Wu et al. (2016)	41.11	37.12
DeepJoint Gharbi et al. (2016)	42.00	39.14
RLDD Guo et al. (2020)	42.49	39.25
DRUNet Zhang et al. (2021)	42.68	39.39
RNAN Zhang et al. (2019b)	43.16	39.70
GRL Li et al. (2023a)	43.57	40.22
KGT (Ours)	43.62	40.68

Evaluation on Image Denoising. We show color and grayscale image denoising results in Tab. 5 under two settings (*i.e.*, † one model for all noise levels $\sigma = \{15, 25, 50\}$ and each model for each noise level). For a fair comparison, both the network complexity and accuracy are reported for all the comparison methods like DnCNN Zhang et al. (2017), FFDNet Zhang et al. (2018a), DRUNet Zhang et al. (2021), RNAN Zhang et al. (2019b), IPT Chen et al. (2021a), EDT Li et al. (2021a), SwinIR Liang et al. (2021), Restormer Zamir et al. (2022), and Xformer Zhang et al. (2023a). For setting †, our KGT achieves better performance on all test datasets for both color and grayscale image denoising compared to all others. It's worth noting that we outperform DRUNet and Restormer with lower trainable parameters. For another setting, our KGT also archives better results on CBSD68 and Urban100 for color image denoising and on Set12 and Urban100 for grayscale denoising. These interesting comparisons validate the effectiveness of the proposed KGT and also indicate that KGT may have a higher generalization. The qualitative results in *Supp. Mat.* also supports that the proposed KGT can remove heavy noise corruption and preserve high-frequency image details.

Evaluation on Image Demosaicking. The quantitative results are shown in 7, which show that the proposed KGT archives the best performance on both the Kodak and MaMaster test datasets. Especially, 0.05dB and 0.45dB absolute improvement compared to the current state-of-the-art GRL.

Evaluation in Adverse Weather Conditions. We validate KGT in adverse weather conditions like rain+fog (Test1), snow (SnowTest100K), and raindrops (RainDrop). The PSNR score is reported in Tab. 6 for each method. It's clear that our method achieves the best performance on Test1 (*i.e.*, 5.76% improvement) and SnowTest100k-L (*i.e.* 8.01% improvement), while the second-best PSNR on RainDrop compared to all other methods. The visual comparison in our *Supp. Mat.*.

Evaluation on SR. For the classical image SR, we compared our KGT with both recent lightweight and accurate SR models, and the quantitative results are shown in Tab. 8. Compared to EDT, KGT-base achieves significant improvements on Urban100 (*i.e.*, 0.72 dB and 0.76dB for x2 and x4 SR) and Manga109 datasets (*i.e.*, 0.22dB and 0.17 dB for x2 and x4 SR). Furthermore, even the KGT-small consistently ranks as the runner-up in terms of performance across the majority of test datasets, all while maintaining a reduced number of trainable parameters. The visual results shown in Fig. 5 also validate the effectiveness of the proposed KGT in restoring more details and structural content.

Evaluation on Image deblurring. Tab. 4 shows the quantitative results for single image motion deblurring on synthetic datasets (GoPro Nah et al. (2017), HIDE Shen et al. (2019)). Compared to

Table 8: ***Classical image SR*** results. Both lightweight and accurate models are summarized.

Method	**Scale**	**Params [M]**	**Set5**		**Set14**		**BSD100**		**Urban100**		**Manga109**	
			PSNR	SSIM	PSNR	SSIM	PSNR	SSIM	PSNR	SSIM	PSNR	SSIM
RCAN Zhang et al. (2018b)	×2	15.44	38.27	0.9614	34.12	0.9216	32.41	0.9027	33.34	0.9384	39.44	0.9786
SAN Dai et al. (2019)	×2	15.71	38.31	0.9620	34.07	0.9213	32.42	0.9028	33.10	0.9370	39.32	0.9792
HAN Niu et al. (2020)	×2	63.61	38.27	0.9614	34.16	0.9217	32.41	0.9027	33.35	0.9385	39.46	0.9785
IPT Chen et al. (2021a)	×2	115.48	38.37	-	34.43	-	32.48	-	33.76	-	-	-
SwinIR Liang et al. (2021)	×2	11.75	38.42	0.9623	34.46	0.9250	32.53	0.9041	33.81	0.9427	39.92	0.9797
CAT-A (Chen et al., 2022b)	×2	16.46	38.51	0.9626	34.78	0.9265	32.59	0.9047	34.26	0.9440	40.10	0.9805
ART Zhang et al. (2023b)	×2	16.40	38.56	0.9629	34.59	0.9267	32.58	0.9048	34.30	0.9452	40.24	0.9808
EDT Li et al. (2021a)	×2	11.48	38.63	0.9632	34.80	0.9273	32.62	0.9052	34.27	0.9456	40.37	0.9811
KGT-S (Ours)	×2	11.87	38.57	0.9651	34.99	0.9300	32.65	0.9078	34.86	0.9472	40.45	0.9824
KGT-B (Ours)	×2	19.90	38.61	0.9654	35.08	0.9304	32.69	0.9084	34.99	0.9455	40.59	0.9830
RCAN Zhang et al. (2018b)	×3	15.63	34.74	0.9299	30.65	0.8482	29.32	0.8111	29.09	0.8702	34.44	0.9499
SAN Dai et al. (2019)	×3	15.90	34.75	0.9300	30.59	0.8476	29.33	0.8112	28.93	0.8671	34.30	0.9494
HAN Niu et al. (2020)	×3	64.35	34.75	0.9299	30.67	0.8483	29.32	0.8110	29.10	0.8705	34.48	0.9500
NLSA Mei et al. (2021)	×3	45.58	34.85	0.9306	30.70	0.8485	29.34	0.8117	29.25	0.8726	34.57	0.9508
IPT Chen et al. (2021a)	×3	115.67	34.81	-	30.85	-	29.38	-	29.49	-	-	-
SwinIR Liang et al. (2021)	×3	11.94	34.97	0.9318	30.93	0.8534	29.46	0.8145	29.75	0.8826	35.12	0.9537
CAT-A (Chen et al., 2022b)	×3	16.64	35.06	0.9326	31.04	0.8538	29.52	0.8160	30.12	0.8862	35.38	0.9546
ART Zhang et al. (2023b)	×3	16.58	35.07	0.9325	31.02	0.8541	29.51	0.8159	30.10	0.8871	35.39	0.9548
EDT Li et al. (2021a)	×3	11.66	35.13	0.9328	31.09	0.8553	29.53	0.8165	30.07	0.8863	35.47	0.9550
KGT-S (Ours)	×3	12.05	34.99	0.9366	31.23	0.8594	29.53	0.8223	30.71	0.8950	35.52	0.9573
KGT-B (Ours)	×3	20.08	35.03	0.9371	31.29	0.8603	29.54	0.8227	30.87	0.9012	35.60	0.9581
RCAN Zhang et al. (2018b)	×4	15.59	32.63	0.9002	28.87	0.7889	27.77	0.7436	26.82	0.8087	31.22	0.9173
SAN Dai et al. (2019)	×4	15.86	32.64	0.9003	28.92	0.7888	27.78	0.7436	26.79	0.8068	31.18	0.9169
HAN Niu et al. (2020)	×4	64.20	32.64	0.9002	28.90	0.7890	27.80	0.7442	26.85	0.8094	31.42	0.9177
IPT Chen et al. (2021a)	×4	115.63	32.64	-	29.01	-	27.82	-	27.26	-	-	-
SwinIR Liang et al. (2021)	×4	11.90	32.92	0.9044	29.09	0.7950	27.92	0.7489	27.45	0.8254	32.03	0.9260
CAT-A (Chen et al., 2022b)	×4	16.60	33.08	0.9052	29.18	0.7960	27.99	0.7510	27.89	0.8339	32.39	0.9285
ART Zhang et al. (2023b)	×4	16.55	33.04	0.9051	29.16	0.7958	27.97	0.751	27.77	0.8321	32.31	0.9283
EDT Li et al. (2021a)	×4	11.63	33.06	0.9055	29.23	0.7971	27.99	0.7510	27.75	0.8317	32.39	0.9283
KGT-S (Ours)	×4	12.02	33.02	0.9082	29.29	0.8026	27.96	0.7582	28.34	0.8467	32.48	0.9322
KGT-B (Ours)	×4	20.04	33.08	0.9090	29.34	0.8037	27.98	0.7599	28.51	0.8467	32.56	0.9335

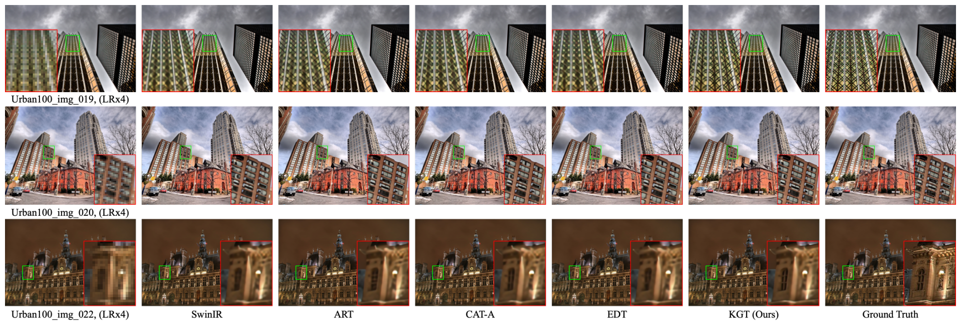

Figure 5: Visual comparison of classical image SR (x4) on Urban100. Best viewed by zooming.

the previous state-of-the-art Restormer Zamir et al. (2022), the proposed KGT achieves significant PSNR improvement of 0.52 dB on the GoPro dataset and the second-best performance with a slightly lower PSNR and SSIM on HIDE dataset. More visual results are shown in the *Supp. Mat.*.

5 Conclusion

In this paper, for the first time, we utilize ViTs from the graph perspective specifically tailored for image restoration with the proposed KGT for both the widely-used multi-stage (for image SR) and the U-shaped architectures (For other IR tasks). In particular, a key graph is constructed that can capture the complex relation of each node feature with only the most relevant K nodes with the proposed Key-Graph constructor instead of a dense fully connected graph. Then the Key-Graph is shared with all the KGT layers within the same KGT stage, which enables the Key-Graph Attention block to capture fewer but the Key relation of each node. As a result, KGT leads to the computation complexity reduced from $\mathcal{O}((hw)^2)$ to $\mathcal{O}((hw) \times K)$, which largely released the potential of ViTs in a sparse yet representative manner. Extensive experiments on 6 IR tasks validated the effectiveness of the proposed KGT and the results demonstrate that the proposed KGT achieves new state-of-the-art performance. The code of the proposed KGT will be released.

REFERENCES

Mark R Banham and Aggelos K Katsaggelos. Digital image restoration. *IEEE signal processing magazine*, 14(2):24–41, 1997.

Christopher M Bishop and Nasser M Nasrabadi. *Pattern recognition and machine learning*, volume 4. Springer, 2006.

Antoni Buades, Bartomeu Coll, and J-M Morel. A non-local algorithm for image denoising. In *2005 IEEE computer society conference on computer vision and pattern recognition (CVPR'05)*, volume 2, pp. 60–65. Ieee, 2005.

Deli Chen, Yankai Lin, Wei Li, Peng Li, Jie Zhou, and Xu Sun. Measuring and relieving the over-smoothing problem for graph neural networks from the topological view. In *Proceedings of the AAAI conference on artificial intelligence*, volume 34, pp. 3438–3445, 2020.

Dexiong Chen, Leslie O'Bray, and Karsten Borgwardt. Structure-aware transformer for graph representation learning. In *International Conference on Machine Learning*, pp. 3469–3489. PMLR, 2022a.

Hanting Chen, Yunhe Wang, Tianyu Guo, Chang Xu, Yiping Deng, Zhenhua Liu, Siwei Ma, Chunjing Xu, Chao Xu, and Wen Gao. Pre-trained image processing transformer. In *Proceedings of the IEEE/CVF Conference on Computer Vision and Pattern Recognition*, pp. 12299–12310, 2021a.

Xiang Chen, Hao Li, Mingqiang Li, and Jinshan Pan. Learning a sparse transformer network for effective image deraining. In *Proceedings of the IEEE/CVF Conference on Computer Vision and Pattern Recognition*, pp. 5896–5905, 2023.

Yinbo Chen, Sifei Liu, and Xiaolong Wang. Learning continuous image representation with local implicit image function. In *Proceedings of the IEEE/CVF conference on computer vision and pattern recognition*, pp. 8628–8638, 2021b.

Zheng Chen, Yulun Zhang, Jinjin Gu, Linghe Kong, Xin Yuan, et al. Cross aggregation transformer for image restoration. *Advances in Neural Information Processing Systems*, 35:25478–25490, 2022b.

Sung-Jin Cho, Seo-Won Ji, Jun-Pyo Hong, Seung-Won Jung, and Sung-Jea Ko. Rethinking coarse-to-fine approach in single image deblurring. In *ICCV*, 2021.

Kostadin Dabov, Alessandro Foi, Vladimir Katkovnik, and Karen Egiazarian. Image denoising by sparse 3-d transform-domain collaborative filtering. *IEEE Transactions on image processing*, 16 (8):2080–2095, 2007.

Tao Dai, Jianrui Cai, Yongbing Zhang, Shu-Tao Xia, and Lei Zhang. Second-order attention network for single image super-resolution. In *IEEE Conference on Computer Vision and Pattern Recognition*, pp. 11065–11074, 2019.

Tri Dao, Daniel Y. Fu, Stefano Ermon, Atri Rudra, and Christopher Ré. FlashAttention: Fast and memory-efficient exact attention with IO-awareness. In *Advances in Neural Information Processing Systems*, 2022.

Alexey Dosovitskiy, Lucas Beyer, Alexander Kolesnikov, Dirk Weissenborn, Xiaohua Zhai, Thomas Unterthiner, Mostafa Dehghani, Matthias Minderer, Georg Heigold, Sylvain Gelly, et al. An image is worth 16x16 words: Transformers for image recognition at scale. In *International Conference on Learning Representations (ICLR)*, 2020.

Max Ehrlich, Larry Davis, Ser-Nam Lim, and Abhinav Shrivastava. Quantization guided jpeg artifact correction. In *European Conference on Computer Vision*, pp. 293–309. Springer, 2020.

Hongyun Gao, Xin Tao, Xiaoyong Shen, and Jiaya Jia. Dynamic scene deblurring with parameter selective sharing and nested skip connections. In *CVPR*, 2019.

Sicheng Gao, Xuhui Liu, Bohan Zeng, Sheng Xu, Yanjing Li, Xiaoyan Luo, Jianzhuang Liu, Xiantong Zhen, and Baochang Zhang. Implicit diffusion models for continuous super-resolution. In *Proceedings of the IEEE/CVF Conference on Computer Vision and Pattern Recognition*, pp. 10021–10030, 2023.

Michaël Gharbi, Gaurav Chaurasia, Sylvain Paris, and Frédo Durand. Deep joint demosaicking and denoising. *ACM Transactions on Graphics (ToG)*, 35(6):1–12, 2016.

Gene H Golub, Per Christian Hansen, and Dianne P O'Leary. Tikhonov regularization and total least squares. *SIAM journal on matrix analysis and applications*, 21(1):185–194, 1999.

Marco Gori, Gabriele Monfardini, and Franco Scarselli. A new model for learning in graph domains. In *Proceedings. 2005 IEEE International Joint Conference on Neural Networks, 2005.*, volume 2, pp. 729–734. IEEE, 2005.

Yu Guo, Qiyu Jin, Gabriele Facciolo, Tieyong Zeng, and Jean-Michel Morel. Residual learning for effective joint demosaicing-denoising. *arXiv preprint arXiv:2009.06205*, 2020.

Kai Han, Yunhe Wang, Jianyuan Guo, Yehui Tang, and Enhua Wu. Vision gnn: An image is worth graph of nodes. *Advances in Neural Information Processing Systems*, 35:8291–8303, 2022.

John Ingraham, Vikas Garg, Regina Barzilay, and Tommi Jaakkola. Generative models for graph-based protein design. *Advances in neural information processing systems*, 32, 2019.

Bo Jiang, Yao Lu, Xiaosheng Chen, Xinhai Lu, and Guangming Lu. Graph attention in attention network for image denoising. *IEEE Transactions on Systems, Man, and Cybernetics: Systems*, 2023.

Jiaxi Jiang, Kai Zhang, and Radu Timofte. Towards flexible blind jpeg artifacts removal. In *Proceedings of the IEEE/CVF International Conference on Computer Vision*, pp. 4997–5006, 2021.

Nicolas Keriven. Not too little, not too much: a theoretical analysis of graph (over) smoothing. *Advances in Neural Information Processing Systems*, 35:2268–2281, 2022.

Filippos Kokkinos, Stamatios Lefkimmiatis, and B A. Iterative joint image demosaicking and denoising using a residual denoising network. *IEEE Transactions on Image Processing*, 28(8): 4177–4188, 2019.

Orest Kupyn, Volodymyr Budzan, Mykola Mykhailych, Dmytro Mishkin, and Jiří Matas. DeblurGAN: Blind motion deblurring using conditional adversarial networks. In *IEEE Conference on Computer Vision and Pattern Recognition*, 2018.

Orest Kupyn, Tetiana Martyniuk, Junru Wu, and Zhangyang Wang. DeblurGAN-v2: Deblurring (orders-of-magnitude) faster and better. In *Proceedings of the IEEE/CVF International Conference on Computer Vision*, 2019.

Yann LeCun, Léon Bottou, Yoshua Bengio, and Patrick Haffner. Gradient-based learning applied to document recognition. *Proceedings of the IEEE*, 86(11):2278–2324, 1998.

Hunsang Lee, Hyesong Choi, Kwanghoon Sohn, and Dongbo Min. Knn local attention for image restoration. In *Proceedings of the IEEE/CVF Conference on Computer Vision and Pattern Recognition*, pp. 2139–2149, 2022.

Juho Lee, Yoonho Lee, Jungtaek Kim, Adam Kosiorek, Seungjin Choi, and Yee Whye Teh. Set transformer: A framework for attention-based permutation-invariant neural networks. In *International conference on machine learning*, pp. 3744–3753. PMLR, 2019.

Wenbo Li, Xin Lu, Jiangbo Lu, Xiangyu Zhang, and Jiaya Jia. On efficient transformer and image pre-training for low-level vision. *arXiv preprint arXiv:2112.10175*, 2021a.

Yawei Li, He Chen, Zhaopeng Cui, Radu Timofte, Marc Pollefeys, Gregory Chirikjian, and Luc Van Gool. Towards efficient graph convolutional networks for point cloud handling. In *Proceedings of the IEEE International Conference on Computer Vision*, pp. 2144–2153, 2021b.

Yawei Li, Yuchen Fan, Xiaoyu Xiang, Denis Demandolx, Rakesh Ranjan, Radu Timofte, and Luc Van Gool. Efficient and explicit modelling of image hierarchies for image restoration. In *Proceedings of the IEEE/CVF Conference on Computer Vision and Pattern Recognition*, pp. 18278–18289, 2023a.

Yawei Li, Kai Zhang, Jingyun Liang, Jiezhang Cao, Ce Liu, Rui Gong, Yulun Zhang, Hao Tang, Yun Liu, Denis Demandolx, et al. Lsdir: A large scale dataset for image restoration. In *Proceedings of the IEEE/CVF Conference on Computer Vision and Pattern Recognition*, pp. 1775–1787, 2023b.

Jingyun Liang, Jiezhang Cao, Guolei Sun, Kai Zhang, Luc Van Gool, and Radu Timofte. Swinir: Image restoration using swin transformer. In *Proceedings of the IEEE/CVF international conference on computer vision*, pp. 1833–1844, 2021.

Bee Lim, Sanghyun Son, Heewon Kim, Seungjun Nah, and Kyoung Mu Lee. Enhanced deep residual networks for single image super-resolution. In *Proceedings of the IEEE Conference on Computer Vision and Pattern Recognition Workshops*, pp. 1132–1140, 2017.

Ding Liu, Bihan Wen, Yuchen Fan, Chen Change Loy, and Thomas S Huang. Non-local recurrent network for image restoration. *Advances in neural information processing systems*, 31, 2018.

Ze Liu, Yutong Lin, Yue Cao, Han Hu, Yixuan Wei, Zheng Zhang, Stephen Lin, and Baining Guo. Swin transformer: Hierarchical vision transformer using shifted windows. In *Proceedings of the IEEE/CVF International Conference on Computer Vision*, pp. 10012–10022, 2021.

Zhilei Liu, Le Li, Yunpeng Wu, and Cuicui Zhang. Facial expression restoration based on improved graph convolutional networks. In *MultiMedia Modeling: 26th International Conference, MMM 2020, Daejeon, South Korea, January 5–8, 2020, Proceedings, Part II 26*, pp. 527–539. Springer, 2020.

Ziwei Luo, Fredrik K Gustafsson, Zheng Zhao, Jens Sjölund, and Thomas B Schön. Image restoration with mean-reverting stochastic differential equations. *arXiv preprint arXiv:2301.11699*, 2023.

Yiqun Mei, Yuchen Fan, and Yuqian Zhou. Image super-resolution with non-local sparse attention. In *IEEE Conference on Computer Vision and Pattern Recognition*, pp. 3517–3526, 2021.

Rafael Molina, Jorge Núñez, Francisco J Cortijo, and Javier Mateos. Image restoration in astronomy: a bayesian perspective. *IEEE Signal Processing Magazine*, 18(2):11–29, 2001.

Chong Mou, Jian Zhang, and Zhuoyuan Wu. Dynamic attentive graph learning for image restoration. In *Proceedings of the IEEE/CVF international conference on computer vision*, pp. 4328–4337, 2021.

Seth A Myers, Aneesh Sharma, Pankaj Gupta, and Jimmy Lin. Information network or social network? the structure of the twitter follow graph. In *Proceedings of the 23rd International Conference on World Wide Web*, pp. 493–498, 2014.

Seungjun Nah, Tae Hyun Kim, and Kyoung Mu Lee. Deep multi-scale convolutional neural network for dynamic scene deblurring. In *Proceedings of the IEEE Conference on Computer Vision and Pattern Recognition*, pp. 3883–3891, 2017.

Ben Niu, Weilei Wen, Wenqi Ren, Xiangde Zhang, Lianping Yang, Shuzhen Wang, Kaihao Zhang, Xiaochun Cao, and Haifeng Shen. Single image super-resolution via a holistic attention network. In *European Conference on Computer Vision*, pp. 191–207, 2020.

Dongwon Park, Dong Un Kang, Jisoo Kim, and Se Young Chun. Multi-temporal recurrent neural networks for progressive non-uniform single image deblurring with incremental temporal training. In *ECCV*, 2020.

Kuldeep Purohit, Maitreya Suin, AN Rajagopalan, and Vishnu Naresh Boddeti. Spatially-adaptive image restoration using distortion-guided networks. In *ICCV*, 2021.

Bin Ren, Yahui Liu, Yue Song, Wei Bi, Rita Cucchiara, Nicu Sebe, and Wei Wang. Masked jigsaw puzzle: A versatile position embedding for vision transformers. In *Proceedings of the IEEE/CVF Conference on Computer Vision and Pattern Recognition*, pp. 20382–20391, 2023a.

Mengwei Ren, Mauricio Delbracio, Hossein Talebi, Guido Gerig, and Peyman Milanfar. Multiscale structure guided diffusion for image deblurring. In *Proceedings of the IEEE/CVF International Conference on Computer Vision*, pp. 10721–10733, 2023b.

William Hadley Richardson. Bayesian-based iterative method of image restoration. *JoSA*, 62(1): 55–59, 1972.

Franco Scarselli, Marco Gori, Ah Chung Tsoi, Markus Hagenbuchner, and Gabriele Monfardini. The graph neural network model. *IEEE transactions on neural networks*, 20(1):61–80, 2008.

MI Sezan and Henry Stark. Image restoration by the method of convex projections: Part 2-applications and numerical results. *IEEE Transactions on Medical Imaging*, 1(2):95–101, 1982.

Ziyi Shen, Wenguan Wang, Xiankai Lu, Jianbing Shen, Haibin Ling, Tingfa Xu, and Ling Shao. Human-aware motion deblurring. In *Proceedings of the IEEE/CVF International Conference on Computer Vision*, pp. 5572–5581, 2019.

Martin Simonovsky and Nikos Komodakis. Dynamic edge-conditioned filters in convolutional neural networks on graphs. In *Proceedings of the IEEE conference on computer vision and pattern recognition*, pp. 3693–3702, 2017.

Maitreya Suin, Kuldeep Purohit, and A. N. Rajagopalan. Spatially-attentive patch-hierarchical network for adaptive motion deblurring. In *CVPR*, 2020.

Xin Tao, Hongyun Gao, Xiaoyong Shen, Jue Wang, and Jiaya Jia. Scale-recurrent network for deep image deblurring. In *CVPR*, 2018.

Zhengzhong Tu, Hossein Talebi, Han Zhang, Feng Yang, Peyman Milanfar, Alan Bovik, and Yinxiao Li. Maxim: Multi-axis mlp for image processing. In *Proceedings of the IEEE/CVF Conference on Computer Vision and Pattern Recognition*, pp. 5769–5780, 2022.

Ashish Vaswani, Noam Shazeer, Niki Parmar, Jakob Uszkoreit, Llion Jones, Aidan N Gomez, Łukasz Kaiser, and Illia Polosukhin. Attention is all you need. In *Advances in Neural Information Processing Systems (NeurIPS)*, 2017.

Xiaolong Wang, Ross Girshick, Abhinav Gupta, and Kaiming He. Non-local neural networks. In *Proceedings of the IEEE conference on computer vision and pattern recognition*, pp. 7794–7803, 2018.

Yinhuai Wang, Jiwen Yu, and Jian Zhang. Zero-shot image restoration using denoising diffusion null-space model. *The Eleventh International Conference on Learning Representations*, 2023.

Yue Wang, Yongbin Sun, Ziwei Liu, Sanjay E Sarma, Michael M Bronstein, and Justin M Solomon. Dynamic graph CNN for learning on point clouds. *Acm Transactions On Graphics (tog)*, 38(5): 1–12, 2019.

Jiqing Wu, Radu Timofte, and Luc Van Gool. Demosaicing based on directional difference regression and efficient regression priors. *IEEE Transactions on Image Processing*, 25(8):3862–3874, 2016.

Keyulu Xu, Chengtao Li, Yonglong Tian, Tomohiro Sonobe, Ken-ichi Kawarabayashi, and Stefanie Jegelka. Representation learning on graphs with jumping knowledge networks. In *International conference on machine learning*, pp. 5453–5462. PMLR, 2018.

Zongsheng Yue, Jianyi Wang, and Chen Change Loy. Resshift: Efficient diffusion model for image super-resolution by residual shifting. *arXiv preprint arXiv:2307.12348*, 2023.

Syed Waqas Zamir, Aditya Arora, Salman Khan, Munawar Hayat, Fahad Shahbaz Khan, Ming-Hsuan Yang, and Ling Shao. Multi-stage progressive image restoration. In *Proceedings of the IEEE/CVF conference on computer vision and pattern recognition*, pp. 14821–14831, 2021.

Syed Waqas Zamir, Aditya Arora, Salman Khan, Munawar Hayat, Fahad Shahbaz Khan, and Ming-Hsuan Yang. Restormer: Efficient transformer for high-resolution image restoration. In *Proceedings of the IEEE/CVF conference on computer vision and pattern recognition*, pp. 5728–5739, 2022.

Hongguang Zhang, Yuchao Dai, Hongdong Li, and Piotr Koniusz. Deep stacked hierarchical multi-patch network for image deblurring. In *CVPR*, 2019a.

Jiale Zhang, Yulun Zhang, Jinjin Gu, Jiahua Dong, Linghe Kong, and Xiaokang Yang. Xformer: Hybrid x-shaped transformer for image denoising. *arXiv preprint arXiv:2303.06440*, 2023a.

Jiale Zhang, Yulun Zhang, Jinjin Gu, Yongbing Zhang, Linghe Kong, and Xin Yuan. Accurate image restoration with attention retractable transformer. In *ICLR*, 2023b.

Kai Zhang, Wangmeng Zuo, Yunjin Chen, Deyu Meng, and Lei Zhang. Beyond a gaussian denoiser: Residual learning of deep cnn for image denoising. *IEEE transactions on image processing*, 26 (7):3142–3155, 2017.

Kai Zhang, Wangmeng Zuo, and Lei Zhang. Ffdnet: Toward a fast and flexible solution for cnn-based image denoising. *IEEE Transactions on Image Processing*, 27(9):4608–4622, 2018a.

Kai Zhang, Yawei Li, Wangmeng Zuo, Lei Zhang, Luc Van Gool, and Radu Timofte. Plug-and-play image restoration with deep denoiser prior. *IEEE Transactions on Pattern Analysis and Machine Intelligence*, 2021.

Kaihao Zhang, Wenhan Luo, Yiran Zhong, Lin Ma, Bjorn Stenger, Wei Liu, and Hongdong Li. Deblurring by realistic blurring. In *CVPR*, 2020.

Yulun Zhang, Kunpeng Li, Kai Li, Lichen Wang, Bineng Zhong, and Yun Fu. Image super-resolution using very deep residual channel attention networks. In *European Conference on Computer Vision*, pp. 286–301, 2018b.

Yulun Zhang, Kunpeng Li, Kai Li, Bineng Zhong, and Yun Fu. Residual non-local attention networks for image restoration. *arXiv preprint arXiv:1903.10082*, 2019b.

Haiyu Zhao, Yuanbiao Gou, Boyun Li, Dezhong Peng, Jiancheng Lv, and Xi Peng. Comprehensive and delicate: An efficient transformer for image restoration. In *Proceedings of the IEEE/CVF Conference on Computer Vision and Pattern Recognition*, pp. 14122–14132, 2023.

Maria Zontak and Michal Irani. Internal statistics of a single natural image. In *CVPR 2011*, pp. 977–984. IEEE, 2011.